







Proceeding Paper

GC-MS Based Metabolite Profiling, and Anti-Inflammatory Activity of Aqueous Extract of *Myrica esculenta* through *In Vitro* and *In Silico* Approach [†]

Amit Kumar Shrivastava ^{1,*} , Dipendra Chaudhary ², Laxmi Shrestha ¹, Maaweya E. Awadalla ³, Samia T. Al-Shouli ⁴ , Anjan Palikhey ¹, Wafa Ali Eltayb ⁵ , Anamika Gupta ⁶, Pramodkumar P. Gupta ^{7,*} , Mala Parab ⁷ , Anchal Trivedi ⁸, Aditi Srivastava ⁸ and Mohnad Abdalla ^{9,*} 

- ¹ Department of Pharmacology, Universal College of Medical Sciences, Bhairahawa 32900, Nepal; drshresthalaxmi@gmail.com (L.S.); anjanpalikhey@gmail.com (A.P.)
- ² Department of Pharmacy, Provincial Lumbini Hospital, Butwal 32907, Nepal; dipendraabc803@gmail.com
- ³ Research Center, King Fahad Medical City, Riyadh Second Health Cluster, Riyadh 11525, Saudi Arabia; mawadalla@kfmc.med.sa
- ⁴ Immunology Unit, Department of Pathology, College of Medicine, King Saud University, Riyadh 11461, Saudi Arabia; salshouli@ksu.edu.sa
- ⁵ Biotechnology Department, Faculty of Science and Technology, Shendi University, Shendi 11111, Sudan; wafa.ali.11338@gmail.com
- ⁶ Cardiovascular Research Group, Sharjah Institute for Medical Research, University of Sharjah, Sharjah 27272, United Arab Emirates; anamikagpt889@gmail.com
- ⁷ School of Biotechnology and Bioinformatics, D Y Patil Deemed to be University, CBD, Belapur, Navi Mumbai 400614, Maharashtra, India; malaparab@gmail.com
- ⁸ Department of Biochemistry, Era's Lucknow Medical College and Hospital, Era University, Lucknow 226003, Uttar Pradesh, India; indiananchaltrivedi@gmail.com (A.T.); aditi1304@gmail.com (A.S.)
- ⁹ Research Institute of Paediatrics, Children's Hospital Affiliated to Shandong University (Jinan Children's Hospital), Jinan 250022, China
- * Correspondence: sr.akshri.ucms.np@gmail.com (A.K.S.); pramodkumar785@gmail.com (P.P.G.); mohnadabdalla200@gmail.com (M.A.)
- [†] Presented at the 2nd International Electronic Conference on Biomedicines, 1–31 March 2023; Available online: <https://ecb2023.sciforum.net/>.



Citation: Shrivastava, A.K.; Chaudhary, D.; Shrestha, L.; Awadalla, M.E.; Al-Shouli, S.T.; Palikhey, A.; Eltayb, W.A.; Gupta, A.; Gupta, P.P.; Parab, M.; et al. GC-MS Based Metabolite Profiling, and Anti-Inflammatory Activity of Aqueous Extract of *Myrica esculenta* through *In Vitro* and *In Silico* Approach. *Med. Sci. Forum* **2023**, *21*, 52. <https://doi.org/10.3390/ECB2023-14079>

Academic Editor: Shaker Mousa

Published: 1 March 2023



Copyright: © 2023 by the authors. Licensee MDPI, Basel, Switzerland. This article is an open access article distributed under the terms and conditions of the Creative Commons Attribution (CC BY) license (<https://creativecommons.org/licenses/by/4.0/>).

Abstract: In the present study was to determine the anti-inflammatory activity of the aqueous extract of the bark and root of *Myrica esculenta* and their active phytoconstituents through *in vitro* and *in silico* studies. The bioactive phytoconstituent of *Myrica esculenta* was determined by GC-MS spectroscopy techniques. After that, total phenolic and flavonoid content of both bark and root extract was determined. Furthermore, *in vitro* anti-inflammatory activity was determined in both extracts. The molecular docking analysis determined the binding affinity of bioactive compounds against inflammatory proteins such as COX-1, COX-2, IL-10, and TNF- α . The present study revealed that bark extract of *Myrica esculenta* has the highest total phenolic and flavonoid content compared with root extract (553.44 ± 18.38 mg GAE/g equivalent and 336.02 ± 8.04 mg quercetin/g equivalent, respectively). Similarly, the bark extract showed good inhibitory activity with 5-LOX and HYA assay (IC_{50} 11.26 ± 3.93 and 21.61 ± 8.27 μ g/mL, respectively), but 15-Lox inhibitory assay root extract showed the highest inhibitory activity, IC_{50} 16.95 ± 5.92 μ g/mL. The docking result showed that myricetin, arjunolic acid, and myricanone have the highest binding affinity with all inflammatory proteins in respective order: myricetin > arjunolic acid > celecoxib > myricanone > myricitrin > 3-epi-ursonic acid. The MD simulation of COX-1 and myricetin showed the highest stability and low deviation at 310 K through RMSD values (1.07 – 2.3 Å) as compared with COX-1 and myricitrin (0.193 – 1.885 Å) and TNF- α and myricanone (1.377 to 3.457 Å), respectively, when analyzed at 100 ns time frame. The extracts and their active constituents showed good anti-inflammatory activity. Further study is essential to define their mechanism of action.

Keywords: *Myrica esculenta*; *in vitro* anti-inflammatory; QSAR analysis; molecular docking; lipoxygenase assay

1. Introduction

Inflammation is the body's defensive mechanism in injured and infected tissues, triggered by immune cells and cytokines that release prostaglandins, interleukin-6, and tumor necrosis factor- α . As inflammatory mediators, inflammatory cytokines have a major role in a variety of disorders, such as asthma, arthritis, gout, etc. Nonsteroidal anti-inflammatory medications (NSAIDs) are primarily used to treat a range of inflammatory diseases and pain associated with such diseases. Anti-inflammatory medicines are thought to be an effective way of reducing the influence of chronic inflammation on the course of degenerative diseases [1]. These drugs, however, possess several side effects that worsen the body mechanism on continuous consumption [2,3]. These challenges generate the need to develop novel pharmaceuticals that are less hazardous and more efficient in treating acute and chronic inflammatory disorders [4]. The adverse effects of non-steroidal anti-inflammatory medicines (NSAIDs) have prompted researchers to examine plant compounds that have potential to develop new anti-inflammatory drug scaffold that can inhibit the release of inflammatory mediators, thereby treating a wide range of disease conditions [5–7].

Myrica esculenta Buch.-Ham. ex D. Don, also recognized as “Hairy Bayberry” and a member of the myricaceae family, is generally referred to as Kaiphala or Kataphala in the north Asian continent and is extensively utilized in Ayurveda for the treatment of several conditions such as asthma, diabetes, gout, arthritis, etc. [8–10]. Numerous species of the myricaceae have been used as medicinal ingredients in traditional medicines from the beginning of time [11]. Scientific research has reported several medicinal perspectives of *Myrica esculenta*, including analgesic, antiasthmatic, antidiabetic, antimicrobial, antihypertensive, antihelmintic, antioxidant, anxiolytic, chemopreventive, antipyretic, antiulcer, and antiulcer, etc. [12,13]. This diverse genus is reported in temperate and sub-tropical regions around the globe [14–16]. The structural diversity of natural products discovered in *Myrica* species put them in a favorable position as possible drug candidates with superior anti-inflammatory capabilities when compared to synthesized compounds [17]. Difficulty in understating complex etiology and exacerbating mechanism leads to hinderance in emergent enchantment bullets for chronic inflammatory disorders. Subsequently, there is a requirement for modern and secure anti-inflammatory agents extracted from plant origin [18].

Introducing protein-ligand docking, computational chemistry allows exploring the plant-inferred molecules as a drug candidate. The majority of recent computational docking approaches presume that the receptor structure is fixed. This allows for the simulated testing of a large number of possible ligands and likely canonical binding sites on receptor molecules. These procedures are significant tools for drug discovery [3]. Furthermore, molecular dynamics (MD) simulations were performed to evaluate the stability of the binding modes established by docking studies in order to investigate the interaction between protein targets and their ligands under settings that are more similar to the physiological environment [19]. The inhibitory potential of molecules presents in *Myrica esculenta* against inflammatory proteins can be established *in vitro* and confirmed via an *in-silico* study, which is cost-effective, time-saving, and can simplify researcher in drug modelling [20].

Thus, keeping in view the significance of the above explanations, the objective of the current study is to assess the anti-inflammatory potential of root and bark extracts of *Myrica esculenta* through *in vitro* evaluation as well as *in silico* molecular docking.

2. Material and Methods

The study was carried out in the department of pharmacology at the Universal College of Medical Sciences, Bhairahawa, Rupandehi, from the month of September 2022 to December 2022 after receiving approval from the Institutional Review Committee (IRC), registration number UCMS/IRC/187/22.

2.1. Plant Collection and Authentication

The bark and root of *Myrica esculenta* were gathered from Tansen, Palpa district, Nepal. The bark and root were cleaned properly with distilled water to remove the dust and shade dried. The collected part of *Myrica esculenta* was authenticated by Mr. Subodh Khanal, Assistant Professor Department of Medicinal and Aromatic plant, Institute of Agriculture and Animal Sciences (IAAS), Paklihawa, Campus, Rupandehi, Nepal (Authentication No: 205/2078/2079).

2.2. Plant Extraction

The bark and root were separately ground and made into coarse powder. The root and bark powders were weighed to 100 g and extracted with distilled water (1:10) separately for 72 h using a continuous hot Soxhlet apparatus. The extracted solvent was collected and dried under a controlled temperature of 70 ± 5 °C in a rotatory evaporator. The semisolid consistency was obtained, both extracts were weighed separately, and the percentage yield was calculated. Both extracts were stored at 4 °C for future use [21]. The % yield was calculated using the formula below:

$$\text{Yield percentage (\%)} = \frac{\text{Weight of extract}}{\text{Weight of Powder}} \times 100 \quad (1)$$

2.3. Total Phenolic Content (TPC)

It was estimated by using the Chludil HD et al., method. The plant extract 2 mg/mL was taken in a volumetric flask with 4.6 mL of distilled water and 0.1 mL of Folin-Ciocalteu reagent was added to it and shaken for 3 min. Then, 0.3 mL of 2% Na₂CO₃ solution was added to the mixture and shaken for 2 h; standard gallic acid solutions (0.1–2 mg/mL) were prepared following the same procedure as the sample. The evaluation was carried out in a triplicate manner, absorbance was measured at 760 nm, and the mean value was calculated [22].

2.4. Total Flavonoid Content (TFC)

The method was based on the Shrivastava AK et al. method. Here, Quercetin was taken as the standard, and its various concentrations were prepared by dissolving it in 70% ethanol and making dilutions (0.1–2 mg/mL). The content was identified using AlCl₃ by the colorimetric method. Standard solution and plant extract were prepared, and 0.2 mL of AlCl₃ (10%), 0.2 mL of potassium acetate (1 M), and 5.6 mL of distilled water were added to both separately, incubated at 37 °C for 30 min. Absorbance was observed at 415 nm under U.V. spectrophotometer, and the standard curve was plotted [23].

2.5. Gas Chromatography and Mass Spectroscopy

The gas chromatography and mass spectroscopy analysis of the aqueous extract of *Myrica esculenta* was performed by the Nepal Academy of Science and Technology (NAST), Kathmandu, Nepal. For this study, an Agilent 7890A GC-Agilent 5975C inert MSD triple axis detector was fitted with an Agilent 19091s-433 (30 m × 250 μM × 0.25 μM) fused column. After that, carrier helium gas was used with an adjusted column velocity of 1 mL/min. The ion source and interface temperature were maintained at 230 and 320 degrees Celsius with applied 6.6018 psi pressure. The 2 μL injector in split mode with a ratio of 75:1 with injection temperature was 230 degrees Celsius. After that, the column temperature was initially maintained at 32 degrees Celsius for 5 min and changed to 70 eV

at a rate of 5 degrees Celsius/minute, respectively. The temperature was increased at 280–320 °C for 5 min. The total elution time was 59.6 min. The relative percentage amount of the compound was evaluated by comparing its average peak area to the total area [24].

2.6. In Vitro Anti-Inflammatory Activity

2.6.1. Lipoygenase (LOX) Inhibition Assay

The LOX inhibition assay of aqueous bark and root extract of *M. esculanta* was evaluated by the previously described method by Truong DH et al., 2020 [25] with minor modification. In the current study, linolic acid and lipoxidase enzyme were used as substrates. The lipoxidase (20,000 U) was dissolved in 1 mL of 0.1 M sodium borate buffer of pH 8.8. The extract was prepared at varying concentrations of 0.1, 0.2, 0.4, 0.8, 1, and 2 mg/mL. The aqueous extract of bark and root of *M. esculanta* at several concentrations was taken in 1 mL portions from each stock in different test tubes. An equal volume of lipoxidase solution was added in each test tube and incubated at 37 °C for 20 min. After the incubation, 1 mL of linolic acid was added to each reaction mixture and mixed. At 234 nm, the absorbance of the reaction mixture was measured with a UV spectrophotometer. Indomethacin and celecoxib were taken as standards. Using the following formula, the percentage of inhibition of LOX activity was determined:

$$\% \text{ inhibition of LOX} = \left[\frac{(A_1 - A_2)}{A_1} \right] \times 100 \quad (2)$$

where A_1 = absorbance of control and A_2 = absorbance of test.

2.6.2. 15-LOX Inhibitory Assay

The 15-LOX inhibitory assay was assessed using the previously described method reported by Adebayo SA et al., 2015. The bark and root extract of *M. esculanta* was prepared at varying concentrations (0.1, 0.2, 0.4, 0.8, 1, and 2 mg/mL). Then, 125 µL of test samples at varying concentrations were added to another test tube. Similarly, 450 µL of 15-LOX was added into the same container and incubated for 15 min at room temperature. After the incubation, 500 µL of linolic acid was added to the reaction mixture and incubated for 15 min at room temperature. The absorbance was measured at 234 nm using UV-visible spectroscopy. The percentage inhibition of 15-LOX was calculated by using the following formula:

$$\% \text{ inhibition of LOX} = \left[\frac{(A_1 - A_2)}{A_1} \right] \times 100 \quad (3)$$

where A_1 = absorbance of control and A_2 = absorbance of test.

2.6.3. Hylurenadase (HYA) Inhibition Assay

The HYA inhibitory activity of bark and root extract of *M. esculanta* was evaluated using a previously defined method reported by Paun G. et al., 2020 [26] after minor modification. The bovine HYA enzyme 100 µL was dissolved in 1 mL (0.1 M) of acetate buffer. The bark and root extracts of *M. esculanta* at varying concentrations of 0.1, 0.2, 0.4, 0.8, 1, and 2 mg/mL were prepared. A 50 µL of extract sample of each concentration was taken into the different test tubes, and then 100 µL of 12.5 mM calcium chloride (CaCl_2) was added to each tube and incubated for 20 min at 37 °C. After the incubation, 250 µL of sodium hyaluronate at 1.2 mg/mL concentration was added to the previous reaction mixture and incubated for 40 min at the same temperature. After the second incubation, 100 µL of sodium hydroxide and potassium borate at 0.4 M was added to the reaction mixture and incubated for 4 min at 90 °C in a water bath. The reaction mixture was then removed from the water bath and allowed to cool at room temperature. Then, 3 mL of 10% of *P*-dimethyl aminobenzyldehyde was added to the cooled reaction mixture, and after 20 min, the absorbance of samples was taken at 585 nm. In the present study, indomethacin

and celecoxib were used as the standards. The HYA inhibition activity was calculated by using the formula as follows:

$$\% \text{ inhibition of HYA} = \left[\frac{(A_1 - A_2)}{A_1} \right] \times 100 \quad (4)$$

where: A_1 = absorbance of control, and A_2 = absorbance of test.

2.7. In Silico Computational Study

2.7.1. Preparation of Target Protein/Macromolecules and Ligands

The selected proteins' 3D X-ray crystal structures (COX1, COX2, TNF- α , and IL-10) were retrieved from the protein data bank server (<https://www.rcsb.org/>) (accessed on 1 September 2021). The protein structure was prepared and purified for molecular docking (Figure 1) [27–29]. The PDB ID of the target proteins were as follows: COX 1 (PDB ID: 4O1Z), COX 2 (PDB ID: 4M11), TNF- α (PDB ID: 2AZ5), and IL-10 (PDB ID 2H24), respectively. In the present study, a total of five phytoconstituents of *Myrica esculenta* were selected from Dr. Duke's phytochemical and ethnobotanical databank (<https://phytochem.nal.usda.gov/phytochem/search/list>) (accessed on 1 October 2021). All the five compounds were selected on the basis of their concentration present in *M. esculenta* plant and their activity. The phytoconstituents were selected in the present study were myricetin (PCID 5281672), myricanone (PCID 161748), 3-epi-ursonic acid (PCID 7163177), myricitrin (PCID 5281673), arjunolic acid (PCID 73641), and celecoxib (PCID 2662), and were obtained from the PubChem database (<https://pubchem.ncbi.nlm.nih.gov/>) (accessed on 1 September 2021) in SDF format and the energy was minimized by using Merck Molecular Force Field (MMFF94) of Chem draw office professional version 16.0. In the present study, celecoxib was selected as the reference compound. The structures of all ligands are represented in Figure 2 [30].

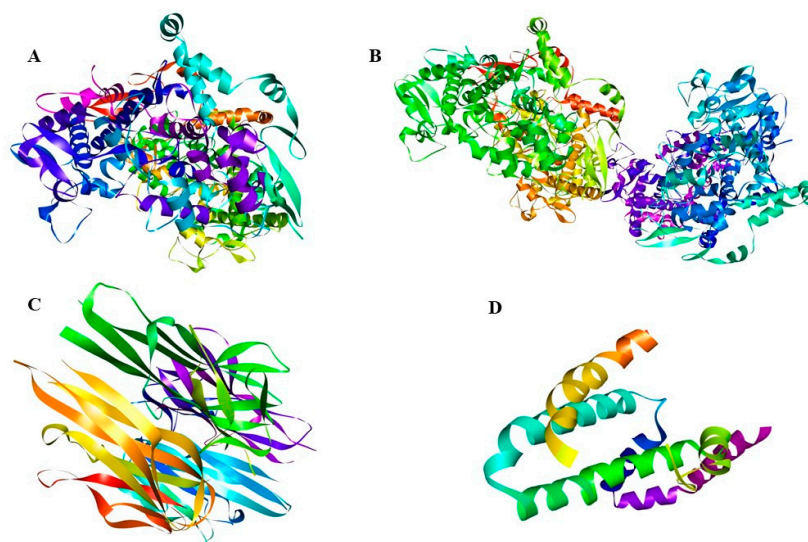


Figure 1. 3D crystal structure of inflammatory proteins (A) cyclooxygenase-1, (B) cyclooxygenase-2, (C) tumor necrosis factor (TNF) alpha, and (D) interleukin-10 (IL-10).

2.7.2. Quantitative Structure-Activity Relationship (QSAR) Analysis

The physio-chemical properties of the investigated substances and their relationship to their biological activity were ascertained using the QSAR analysis. Version 8.0.3 of the Hyper Cam Professional utility was used for the QSAR analysis. First, using the semi-empirical PM3 approach, the individual compound's structure was optimized. Subsequently, energy was reduced using the Fletcher-Reeves conjugate gradient algorithm. Several QSAR parameters were evaluated in this investigation, including free energy, hydration energy, total energy, refractivity, surface area, volume polarizability, mass, dipole movement, and log P [31,32].

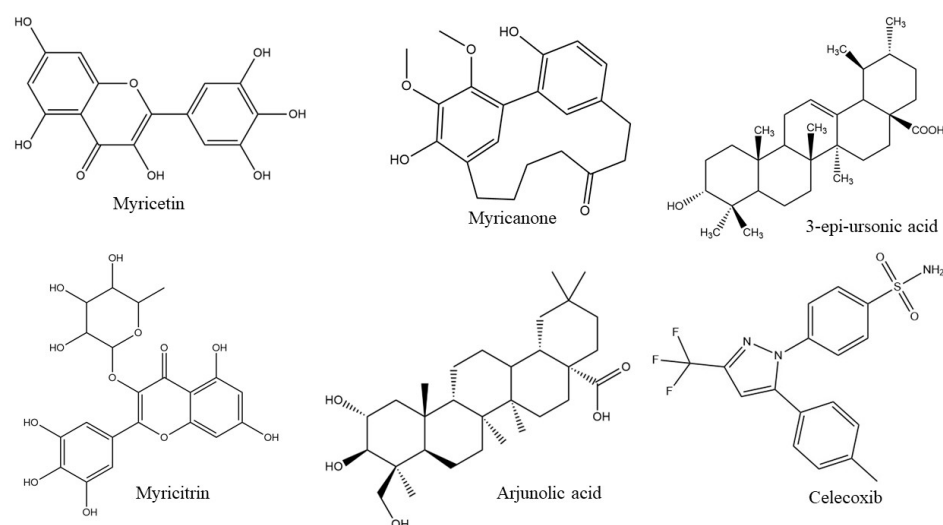


Figure 2. Structure of different phytoconstituent of *Myrica esculenta*.

2.7.3. Molecular Docking Analysis

2.7.3.1. AutoDock 4.2.6

Molecular docking of chosen five phytoconstituents of *M. esculenta* and the reference drug celecoxib was carried out using AutoDock version 4.2.6 against four inflammatory proteins (COX1, COX2, TNF- α , and IL-10) (<http://autodock.scripps.edu/>) (accessed on 15 November 2021). With a grid spacing of 0.375 and grid coordinates in the X, Y, and Z axes set to $60 \times 60 \times 60$, the native ligand's position on the protein's binding site was determined using auto-grid. The search was conducted using the Lamarckian genetic algorithm with a total of 10 iterations of GA criteria, and the binding energies of the results were further examined. Based on the lowest binding energy (B.E.) and inhibition constant (K_i), the optimal possible orientation of the ligand in the protein binding pocket was computationally analyzed and visualized using Accelrys Biovia Discovery studio version 17.1 [28,33].

2.7.3.2. AutoDock Vina

In the present study, AutoDock vina (<http://vina.scripps.edu/>) (accessed on 18 November 2021) version 2.1 was used to validate the docking procedure of AutoDock 4.2. It is significantly faster and more accurate in predicting the ligand-binding pocket than AutoDock 4.2. It uses multithread on multicore machines, resulting in faster results and automatically calculates the grid maps and clusters. It is used to run docking simulations, producing ten confirmations of ligand and protein complexes and ranking them based on binding energy and RMSD values. Visualization of the confirmation was carried out using Accelrys Biovia Discovery studio version 2020 [34].

2.7.3.3. iGMDOCK

Another docking software, iGMDOCK version 2.1, was used to bind the protein and ligands. The following are the genetic algorithm parameters that help in docking process: the population size is 200, the generations are 70, and the number of solutions is 2. Following the generation of the poses library, the best match was chosen to represent the overall binding energy in the form of hydrogen bonds (HB), van der Waals forces (VDW), and electrostatic interactions (EI) [35].

2.7.4. Molecular Dynamic Simulation

2.7.4.1. LARMD Online Server

Ligand-driven protein molecular dynamics analysis in drug development offers the best comprehension of how a protein functions in a physiological system. MD simulation

of myricitrin with COX-1 (PDB ID: 4O1Z) and myricanone with TNF- α (PDB ID: 2AZ5) were conducted using ligand and receptor molecular dynamic (LARMD) web application version 1.0. (<http://chemyang.ccnu.edu.cn/ccb/server/LARMD/>) (accessed on 17 December 2021). To analyze receptor-ligand interactions at the atomic level, the LARMD server employs three modules: traditional molecular dynamics (Int mod), normal mode analysis (Nor mod), and steered molecular dynamics simulations (Str mod). Frequently used programs including CAVER3.0, AMBER16, MDTraj, and Bio3d are included in these three modules. JSmol, Chart.js, and MolScript are only a few of the plugins and programs that are integrated to show and evaluate the outcome on the Web page.

When employing molecular docking, the optimal binding poses of myricetin and myricitrin with COX-1 (PDB ID: 4O1Z) and myricanone with TNF- (PDB ID: 2AZ5) were uploaded in the initial stage to the PDB2PQR server, which generated the electrostatic fields of the receptor under various pH values. The MD simulation time was optimized for 3 ns by using the advanced settings. Following the first task submission of the ligand-receptor complex file, the ligand and non-standard residue(s) were enrolled for energy calculations and trajectory analysis. The service provided molecular dynamics simulation results in components such as PCA, conformation cluster, dynamic residue cross-correlations, hydrogen bond analysis, binding free energy, and energy decomposition. Standard molecular dynamics simulation module (Int mod) and steered molecular dynamics simulation module (Str mod) were utilized to investigate the interaction and dynamics of the inflammatory protein-ligand [36,37].

2.7.4.2. MD Simulation Methodology Using Schrodinger Software

The docking poses of myricetin-COX-1, myricitrin-COX-1, and myricanone-TNF- α and complexes that had lowest binding energies were chosen for molecular dynamic simulation for the determination of their docking complexes stability by employing the Desmond module of Schrodinger LCC computational software (Schrodinger, München, Germany) and the VMD molecular dynamic simulation tool was also used. Using the Desmond system builder, a water-soaked solvated system was constructed. A solvation system was thought to exist in the TIP3P water model system. The orthorhombic box has a periodic boundary condition of buffer distance, that has to be at least 10 Å from the protein's surface. The MD simulation was carried out using the OPLS-3e force field, and the simulation box was filled with 0.15 M sodium chloride (NaCl) to preserve the iso-osmotic condition. A predetermined equilibrium protocol was executed prior to the simulation. Following the simulation's equilibration, the abandoned production phase was conducted under NPT ensemble for 100 ns at 310 K and 1.01325 bar pressure. During the 100 ns MD simulation, 1000 frames were generated and recorded to the trajectory. Following the MD simulation, the interaction picture was utilized to examine the trajectory of the simulation using RMSD, RMSF, hydrogen bond analysis, and radiation of gyration (rg) [38–40].

2.7.4.3. Statistical Analysis

The *in vitro* anti-inflammatory activity values were calculated and represented in mean \pm SEM. Microsoft Excel 2010 was used to obtain the % inhibition and IC50 values.

3. Results

3.1. Extractive Value of Bark and Root Extract of *Myrica esculenta* Plant

Percentage yield of Bark extract = 24.76%.

$$\% \text{ yield of bark extract} = \frac{12.38}{50} \times 100 \quad (5)$$

Percentage yield of root extract = 21.92%.

$$\% \text{ yield of root extract} = \frac{10.96}{50} \times 100 \quad (6)$$

3.2. Determination of Total Phenolic and Total Flavonoid Content

Myrica esculenta has a considerable concentration of phenolic and flavonoid content in its aqueous bark and root extract. The total phenolic and flavonoid content was concentration dependent. The mean phenolic content of bark and root extract was 553.44 ± 18.38 and 421.17 ± 5.34 GAE/g equivalent, respectively. The total content of flavonoid in bark and root extract was 336.02 ± 8.04 and 277.65 ± 2.42 quercetin/g equivalent, respectively. The result indicated that the bark extract of *M. esculenta* has the highest TPC and TFC content compared to the root extract (Table 1).

Table 1. The mean TPC content of *Myrica esculenta* bark and root extract was 553.44 ± 18.38 and 421.17 ± 5.34 mg GAE/g equivalent, respectively. The mean TFC content of bark and root extract of *Myrica esculenta* was 336.02 ± 8.04 and 277.65 ± 2.42 mg quercetin/g equivalent, respectively. The value was expressed in mean \pm SEM.

Conc. (mg/mL)	Mean Absorbance of TPC at 765 nm and TFC at 510 nm											
	Bark Extract						Root Extract					
	Abs. of Ex- tract	Conc. of Gallic Acid (mg/mL)	TPC (mg GAE/g)	Abs. of Ex- tract	Conc. of Quercetin (mg/mL)	TFC (mg of Quercetin/g)	Abs. of Ex- tract	Conc. of Gallic Acid (mg/mL)	TPC (mg GAE/g)	Abs. of Ex- tract	Conc. of Quercetin (mg/mL)	TFC (mg of Quercetin/g)
0.1	0.332	28.63 \pm 1.14	286.34 \pm 11.40	0.238	15.84 \pm 0.09	158.40 \pm 0.98	0.245	21.06 \pm 0.05	210.69 \pm 0.50	0.168	11.11 \pm 0.12	111.10 \pm 1.25
0.2	0.459	39.70 \pm 2.06	397.07 \pm 20.61	0.353	23.94 \pm 0.26	239.48 \pm 2.65	0.317	27.38 \pm 1.10	273.88 \pm 11.06	0.289	19.28 \pm 0.30	191.28 \pm 3.03
0.4	0.560	51.67 \pm 2.26	484.89 \pm 22.63	0.452	29.10 \pm 0.05	291.05 \pm 5.85	0.462	39.96 \pm 0.77	399.68 \pm 7.78	0.379	25.34 \pm 0.28	253.44 \pm 2.81
0.8	0.688	56.54 \pm 2.01	596.20 \pm 20.15	0.571	38.31 \pm 0.64	387.455 \pm 6.41	0.533	46.14 \pm 0.28	461.42 \pm 2.85	0.477	32.01 \pm 0.21	320.11 \pm 2.14
1.0	0.841	71.15 \pm 1.47	729.24 \pm 14.74	0.682	45.97 \pm 2.90	459.75 \pm 29.07	0.627	54.31 \pm 0.27	543.15 \pm 2.76	0.529	35.52 \pm 0.45	355.06 \pm 4.52
2.0	0.953	82.69 \pm 2.07	826.92 \pm 20.76	0.714	47.97 \pm 0.33	480.02 \pm 3.31	0.736	63.82 \pm 0.71	638.23 \pm 7.10	0.645	43.31 \pm 0.07	433.17 \pm 0.78
Mean \pm SEM			553.44 \pm 18.38			336.02 \pm 8.04			421.17 \pm 5.34			277.65 \pm 2.42

3.3. Identification of Phytoconstituents by GC-MS Analysis

In the current work, GC-MS analysis of an aqueous extract of *M. esculenta* bark was used to predict a total of 21 bioactive components. Figure 3 depicts the GC-MS spectra, while Table 2 provides the retention time, molecular formula, molecular weight, and concentration. The bioactive compounds present in the aqueous extract of *Myrica esculenta* bark are as follows: methyl salicylate, O-amino benzohydroxamic acid, pyridine, 4-(1,1-dimethylethyl)-, benzoic acid, 4-amino-, hydrazide, 1,2,4-triazolo(4,3-a) pyrimidine, 2-chlorobenzimidazole, 5-chlorobenzimidazole, benzenemethanamine, N-methyl-, 2-isocyanatopyridine, N,N,N',N'-tetraethyl-1,2-di-furan-2-yl-ethane-1,2-diamine, eicosane, octadecane, tetratetracontane, hexatriacontane, docosane, 7-hexyl-, tetrapentacontane, triacontane, 1-bromo-, hentriacontane, tetracosane, octadecane, 3-ethyl-5-(2-ethylbutyl)-, and dotriacontane.

3.4. In Vitro Anti-Inflammatory Activity

In vitro anti-inflammatory efficacy of an aqueous extract of the bark and root of *M. esculenta* is depicted in Table 3. The result showed that bark extract has significant inhibition of 5-Lox, 15-Lox, and HYA which were 11.26 ± 3.93 , 25.57 ± 8.94 , and 21.61 ± 8.27 μ g/mL, respectively. Root extract has good inhibition but is least effective compared to bark extract, except 15-Lox inhibition which was 16.95 ± 5.92 μ g/mL. Similarly, 5-Lox and HYA inhibition were 23.024 ± 8.04 and 40.24 ± 15.41 μ g/mL, respectively. The present study used two standard anti-inflammatory drugs, indomethacin and celecoxib. In comparison between both standard drugs, indomethacin showed the highest inhibition in 5-Lox (9.87 ± 3.78 μ g/mL), 15-Lox (12.19 ± 4.67 μ g/mL), and HYA (7.82 ± 2.99 μ g/mL) activities, respectively.

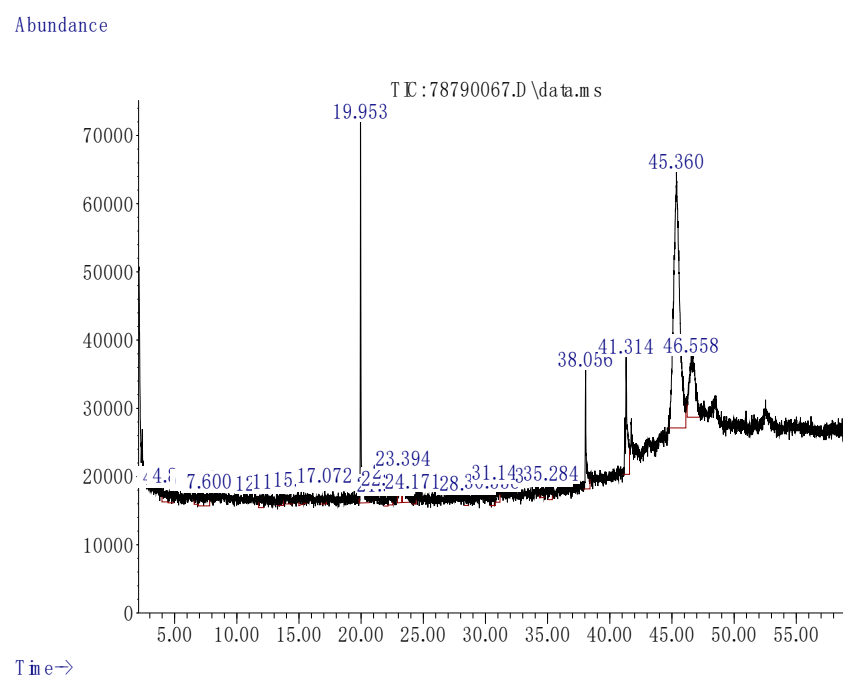


Figure 3. GC-MS spectra of *Myrica esculenta* bark extract.

Table 2. Determination of Bioactive compounds present in aqueous bark extract of *Myrica esculenta*.

S.N.	RT (min)	Peak Width 50% (min)	Compound Name	Molecular Formula	Molecular Weight	Structure
1	4.094	0.485	Methyl salicylate	C ₈ H ₈ O ₃	152.047	
2	4.86	0.485	O-Amino benzohydroxamic acid	C ₇ H ₈ N ₂ O ₂	152.059	
3	6.672	0.324	Pyridine, 4-(1,1-dimethylethyl)-	C ₁₁ H ₁₇ NS	135.105	
4	7.147	0.432	Benzoic acid, 4-amino-, hydrazide	C ₇ H ₉ N ₃ O	151.075	
5	7.6	0.486	1,2,4-Triazolo(4,3-a)pyrimidine	C ₅ H ₄ N ₄	120.044	

Table 2. Cont.

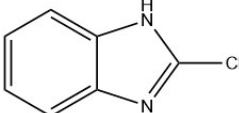
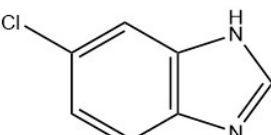
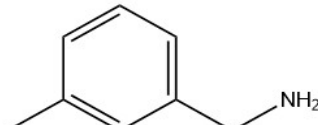
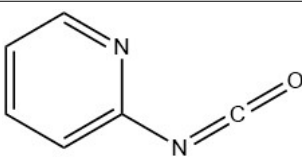
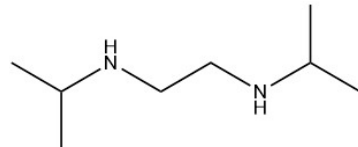





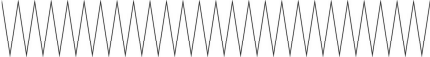



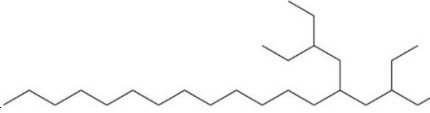

S.N.	RT (min)	Peak Width 50% (min)	Compound Name	Molecular Formula	Molecular Weight	Structure
6	12.12	0.432	2-Chlorobenzimidazole	C ₇ H ₅ ClN ₂	152.014	
7	13.501	0.486	5-Chlorobenzimidazole	C ₇ H ₅ ClN ₂	152.014	
8	14.343	0.593	Benzenemethanamine, N-methyl-	C ₈ H ₁₁ N	121.089	
9	15.184	0.593	2-Isocyanatopyridine	C ₆ H ₄ N ₂ O	120.032	
10	17.072	0.486	N,N,N',N'-Tetraethyl-1,2-di-furan-2-yl-ethane-1,2-diamine	C ₄ H ₁₂ N ₂	304.215	
11	19.953	0.863	Eicosane	C ₂₀ H ₄₂	282.329	
12	21.916	0.378	Octadecane	C ₁₈ H ₃₈	254.297	
13	22.251	0.378	Tetratetracontane	C ₄₄ H ₉₀	618.704	
14	23.179	0.378	Hexatriacontane	C ₃₆ H ₇₄	506.579	
15	24.171	0.378	Docosane, 7-hexyl-	C ₂₈ H ₅₈	394.454	
16	28.541	0.378	Tetrapentacontane	C ₅₄ H ₁₁₀	758.861	
17	30.558	0.432	Triacontane, 1-bromo-	C ₃₀ H ₆₀ Br	500.396	
18	31.141	0.378	Hentriacontane	C ₃₁ H ₆₄	436.501	
29	38.056	0.539	Tetracosane	C ₂₄ H ₅₀	338.391	
20	41.314	0.539	Octadecane, 3-ethyl-5-(2-ethylbutyl)-	C ₂₆ H ₅₄	366.423	
21	46.558	1.025	Dotriacontane	C ₃₂ H ₆₆	450.516	

Table 3. *In vitro* anti-inflammatory activity of aqueous bark and root extract of *Myrica esculenta*.

	5-LOX (IC ₅₀)	15-LOX (IC ₅₀)	HYA (IC ₅₀)
Bark extract	11.26 ± 3.93	25.57 ± 8.94	21.61 ± 8.27
Root extract	23.024 ± 8.04	16.95 ± 5.92	40.24 ± 15.41
Indomethacin	9.87 ± 3.78	12.19 ± 4.67	7.82 ± 2.99
Celecoxib	14.07 ± 5.38	8.62 ± 3.30	17.96 ± 6.87

3.5. *In Silico* Computational Analysis

3.5.1. Quantitative Structure–Activity Relationship (QSAR) Studies

The current study's computational QSAR analysis discovered that the partition coefficient (log P) values of 3-epi-ursolic acid were 9.37 greater than those of other substances. The increase in the log *p* value indicated the ability to permeate into the biological membrane, particularly the blood brain barrier (BBB), exhibiting its neurological activity. The other key parameters of all selected compounds were also estimated and reported in Table 4.

Table 4. QSAR study of selected compounds.

Function	3-Epi-Ursolic Acid	Arjunolic Acid	Celecoxib	Myricetin	Myricanone	Myricitrin
Surface area (Approx) (Å ²)	539.38	592.70	529.12	395.28	450.85	523.82
Surface area (Grid) (Å ²)	649.10	680.61	595.51	485.46	550.54	644.51
Volume (Å ³)	1239.43	1323.95	987.13	802.37	993.22	1138.09
Hydration energy (Kcal/mole)	−4.67	−11.58	−10.90	−40.64	−12.50	−45.17
Log P	9.37	7.84	7.86	4.05	5.51	3.27
Refractivity (Å ³)	122.50	132.91	37.41	20.81	52.62	51.96
Polarizability (Å ³)	53.12	54.59	32.80	29.18	38.47	41.96
Mass (amu)	456.71	490.72	381.37	318.24	356.42	464.38
Total energy (kcal/mol)	74.3512	109.971	45.3604	7.90082	22.7156	22.8694
Dipole moment (Debye)	1.766	0	2.792	3.297	1.536	0
RMS gradient (kcal/Å mol)	0.09703	0.09558	0.09688	0.0953	0.09526	0.09747

3.5.2. Molecular Docking

Molecular docking analysis of selected *M. esculenta* phytoconstituents (myricetin, myricanone, 3-epi-ursolic acid, myricitrin, arjunolic acid) and a reference drug celecoxib were carried out against four selected inflammatory proteins (COX1, COX2, TNF- α , and IL-10) using AutoDock v4.2.6. In order to gather the binding energy necessary for complex formation and examine the molecular processes underlying the inhibition of particular proteins, the catalytically active region of proteins was targeted. Tables 5 and 6 represent a summary of the binding energies and dissociation constants (K_d) of *M. esculenta* phytoconstituents with regard to the above-mentioned proteins. The result was further validated using AutoDock vina and iGEMDOCK expressed in Tables 7–10 respectively. The results analyzed from AutoDock v4.2.6 showed that all the five phytoconstituents and standard drug celecoxib exhibited potent binding affinity to inflammatory proteins.

The binding affinities of the phytoconstituents and reference drug (celecoxib) with cyclooxygenase-1 (PDB ID: 4O1Z) decreased in order myricetin > arjunolic acid > celecoxib > myricanone > myricitrin > 3-epi-ursolic acid. However, myricetin (BE = −9.95 kcal/mol, k_d = 50.71 nM) and arjunolic acid (BE = −9.25 kcal/mol, k_d = 165.34 nM) were shown to have greater binding affinity than standard drug celecoxib (BE = −7.9 kcal/mol, k_d = 1.61 μ M) (Table 5). The binding affinities with cyclooxygenase-2 (PDB ID: 4M11) decreased in the order myricetin > arjunolic acid > 3-epi-ursolic acid > myricanone > celecoxib > myricitrin. The binding affinities of all the phytoconstituents except myricitrin were found to be similar to that of the reference drug celecoxib (BE = −5.72 kcal/mol, k_d = 64.32 μ M) with myricetin (BE = −6.97 kcal/mol, k_d = 7.79 μ M) and arjunolic acid (BE = −6.92 kcal/mol, k_d = 8.5 μ M).

showing highest affinities (Table 4). Analysis utilizing AutoDock Vina and the iGEMDOCK program further confirmed the outcome (Table 7).

Table 5. Binding energies (kcal/mol) and dissociation constants (K_d) of myricetin, myricanone, 3-epi-ursonic acid, myricitrin, arjunolic acid, and celecoxib towards COX-1 and COX-2 using AutoDock 4.2.6.

S.N.	Ligands	COX-1 (PDB ID: 4O1Z)				COX-2 (PDB ID: 4M11)			
		B.E. (kcal/mol)	Diss. Constant (K_d)	Interacting Amino Acid	H-Atom	B.E. (kcal/mol)	Diss. Constant (K_d)	Interacting Amino Acid	H-Atom
1.	Myricetin	−9.95	50.71 nM	Ser143, Arg374, Asn375, Gly533, Gly533, Asn537, Asn537, Asn53, Val228, Val228, Val228, Gly227	6	−6.97	7.79 μ M	Phe361, Phe36, Lys360, Trp545, Arg61	4
2.	Myricanone	−7.65	2.46 μ M	Ser143, Trp139, Arg376, Arg37	1	−6.51	16.78 μ M	Trp545, Asp362, Asn560	2
3.	3-epi-ursonic acid	−6.88	9.08 μ M	Arg376, Asn375, Gly225	2	−6.72	11.89 μ M	Asp239, His242, Lys253	3
4.	Myricitrin	−7.64	2.51 μ M	Asp229, Trp139, Ser143, Arg376, Phe142, Arg374, Val145, Asn375	6	−4.37	624.03 μ M	Glu346, Arg109, Lys342, Glu553, Trp545, Asp362, Lys360	-
5.	Arjunolic acid	−9.25	165.34 nM	Arg374, Asn375, Asn537, Val228, His226, Val145, Phe142	1	−6.92	8.5 μ M	Arg61, Asn560	-
6.	Celecoxib	−7.9	1.61 μ M	Asn375, Asn37, Asn375, Trp139, Ser143, Arg374, Gly225	1	−5.72	64.32 μ M	Lys342, Lys360, Lys557, Glu553, Glu553	1

Table 6. Binding energies (kcal/mol) and dissociation constants (K_d) of myricetin, myricanone, 3-epi-ursonic acid, myricitrin, arjunolic acid, and celecoxib towards TNF- α and IL-10 using AutoDock 4.2.6.

S.N.	Ligands	Tumor Necrosis Factor (TNF)- α (PDB ID: 2AZ5)				Interleukin (IL)-10 (PDB ID: 2H24)			
		B.E. (kcal/mol)	Diss. Constant (K_d)	Interacting Amino Acid	H-Atom	B.E. (kcal/mol)	Diss. Constant (K_d)	Interacting Amino Acid	H-Atom
1.	Myricetin	−7.3	4.42 μ M	Lys11, Lys11	2	−5.78	57.5 μ M	Arg110, Phe111, Phe56	1
2.	Myricanone	−7.78	2.0 μ M	Gly121	2	−7.09	6.32 μ M	Phe56, Phe111	2
3.	3-epi-ursonic acid	−6.97	7.84 μ M	Leu120, Ser60	-	−4.51	491.31 μ M	Arg102, Arg102, Arg106, Gln70	1
4.	Myricitrin	−5.55	85.03 μ M	Ser60, Gln61, Leu120	-	−5.09	184.36 μ M	Glu74, Arg102, Glu115, Gln63	-
5.	Arjunolic acid	−7.34	4.2 μ M	Leu120, Leu57	-	−6.76	11.11 μ M	Gly61, Gly58, Cys62	-
6.	Celecoxib	−6.52	16.55 μ M	Tyr59, Tyr59, Tyr151, Tyr151, Tyr151, Gln61	-	−5.44	102.12 μ M	Glu115, Asn116, Arg102, Arg102, Gln70, Glu74	1

The binding affinities of phytoconstituents and celecoxib with tumor necrosis factor (TNF- α) (PDB ID: 2AZ5) decreased in the following order: myricanone > arjunolic acid > myricetin > 3-epi-ursonic acid > celecoxib > myricitrin, as shown in Table 6. Similar binding affinities of phytoconstituents except myricitrin were found with TNF- α protein having the highest affinity of myricanone (BE = −7.78 kcal/mol, k_d = 2.0 μ M) as compared to celecoxib (BE = −6.52 kcal/mol, k_d = 16.55 μ M). Similarly, myricanone showed the highest affinity towards interleukin (IL)-10 (PDB ID: 2H24) (BE = −7.09 kcal/mol, k_d = 6.32 μ M) as compared to celecoxib (BE = −5.44 kcal/mol, k_d = 102.12 μ M), respectively. The results were further confirmed using AutoDock vina (Table 8) and iGEMDOCK (Tables 9 and 10).

Table 7. Binding energies (kcal/mol) and dissociation constants (K_d) of myricetin, myricanone, 3-epi-ursonic acid, myricitrin, arjunolic acid, and celecoxib towards COX-1 and COX-2 using AutoDock vina.

S.N.	Ligands	COX-1 (PDB ID: 4O1Z)			COX-2 (PDB ID: 4M11)		
		B.E. (kcal/mol)	Diss. Constant (K_d)	Interacting Amino Acid	B.E. (kcal/mol)	Diss. Constant (K_d)	Interacting Amino Acid
1.	Myricetin	−9.7	79.61 nM	Cys47,His43,Gln44,Gln461	−9.9	53.8 nM	Cys41, Arg44, Gln461
2.	Myricanone	−8.4	290.78 nM	Gln372,Glu543	−8.9	314.99 nM	Gln543,Arg44
3.	3-epi-ursonic acid	−9.3	150.85 nM	Asp135,Gln327, Arg157	−9.2	181.8 nM	Gln372,Gln370, Gln543, Arg44
4.	Myricitrin	−10.1	38.59 nM	Gln327, Asn34, Asp135	−10.5	13.51 nM	Glu322, Val132
5.	Arjunolic acid	−9.0	229.41 nM	Asn34, Arg157	−9.5	109.5 nM	Gly225, Tyr373
6.	Celecoxib	−9.5	102.91 nM	Lys532,Gln372,Pro542, Arg61, Lys546	−9.3	150.85 nM	Tyr130, Cys41

Table 8. Binding energies (kcal/mol) and dissociation constants (K_d) of myricetin, myricanone, 3-epi-ursonic acid, myricitrin, arjunolic acid, and celecoxib towards TNF- α and IL-10 using AutoDock vina.

S.N.	Ligands	Tumor Necrosis Factor (TNF)- α (PDB ID: 2AZ5)			Interleukin (IL)-10 (PDB ID: 2H24)		
		B.E. (kcal/mol)	Diss. Constant (K_d)	Interacting Amino Acid	B.E. (kcal/mol)	Diss. Constant (K_d)	Interacting Amino Acid
1.	Myricetin	−7.8	1.91 μ M	Ser95,Arg82	−6.3	24.29 μ M	Arg110, Cys62
2.	Myricanone	−8.2	945.3 nM	Tyr151, Tyr59	−8.0	1.62 μ M	Phe56, Phe111
3.	3-epi-ursonic acid	−9.2	181.81 nM	Leu157	−7.4	3.95 μ M	Arg106, Arg102
4.	Myricitrin	−8.0	9.95 μ M	Gly121,Tyr151	−6.8	11.55 μ M	Ala139
5.	Arjunolic acid	−9.4	120.71 nM	Tyr151,Gly121, Leu120	−8.3	848.93 nM	Gln63, Glu67
6.	Celecoxib	−8.2	945.3 nM	Gln125, Gly121	−8.1	1.1 μ M	Phe30

Table 9. Binding energies (kcal/mol) and dissociation constants (K_d) of myricetin, myricanone, 3-epi-ursonic acid, myricitrin, arjunolic acid, and celecoxib towards COX-1 and COX-2 using iGEMDOCK.

S.N.	Ligands	COX-1 (PDB ID: 4O1Z)				COX-2 (PDB ID: 4M11)			
		T.E. (kcal/mol)	vDW	HB	E.I.	T.E. (kcal/mol)	vDW	HB	E.I.
1.	Myricetin	−132.492	−105.267	−27.2253	0	−125.784	−91.263	−34.5206	0
2.	Myricanone	−87.3133	−75.4082	−11.9051	0	−107.541	−97.6307	−9.90984	0
3.	3-epi-ursonic acid	−103.976	−87.1912	−16.4963	−0.288703	−86.4932	−69.4132	−17.08	0
4.	Myricitrin	−125.517	−93.0059	−32.5107	0	−114.496	79.4543	−35.0418	0
5.	Arjunolic acid	−83.2344	−67.5726	−15.6618	0	−87.3774	−71.8736	−15.5038	0
6.	Celecoxib	−108.282	−100.838	−7.44436	0	−90.8942	−83.167	−7.72725	0

The docking validation was assessed with AutoDock vina. In Table 6, the result expressed that myricitrin has the highest and almost equal binding affinity with COX-1 and COX-2 protein (BE = −10.1 kcal/mol, k_d = 38.59 and BE = −10.5 kcal/mol, k_d = 13.51), respectively. In contrast, other phytoconstituents of *M. esculenta* showed almost similar interaction. The arjunolic acid and 3-epi ursonic acid have the highest interaction with TNF- α (−9.4 Kcal/mol k_d 120.71 nm and −9.2 Kcal/mol, k_d 181.81 nm), respectively. Similarly, myricanone (−8.0 Kcal/mol, k_d 1.62 μ M) and arjunolic acid (−8.3 Kcal/mol, k_d 848.93 nM) showed the highest and equal binding affinity with IL-10 (Table 7). The selected inflammatory proteins were redocked with active phytoconstituents of *M. esculenta* using iGEMDOCK v 2.1. The result revealed that myricetin shows strong interaction with COX-1 (−125.784 Kcal/mol) and COX-2 (−132.492 Kcal/mol) in Table 9, respectively. Whereas with TNF- α , myricitrin (−108.99), arjunolic acid (−95.38), and myricetin (−91.44)

showed the highest interaction. Similarly, IL-10 myricetin and myricitrin showed strong interaction with binding energies -87.17 and -86.14 Kcal/Mol, respectively, in Table 10. The ligand-protein interaction by different docking tools were visualized in Supplementary Tables S1–S4.

Table 10. Binding energies (kcal/mol) and dissociation constants (K_d) of myricetin, myricanone, 3-epi-arjunolic acid, myricitrin, arjunolic acid, and celecoxib towards TNF- α and IL-10 using iGEMDOCK.

S.N.	Ligands	Tumor Necrosis Factor (TNF)- α (PDB ID: 2AZ5)				Interleukin (IL)-10 (PDB ID: 2H24)			
		T.E. (kcal/mol)	vDW	HB	E.I.	T.E. (kcal/mol)	vDW	HB	E.I.
1.	Myricetin	-91.4497	-65.7845	-25.6652	0	-75.9232	-60.0728	-15.8504	0
2.	Myricanone	-87.7068	-73.3761	-14.3307	0	-77.8226	-68.6794	-9.14318	0
3.	3-epi-arjunolic acid	-85.9916	-78.5542	-7.43742	0	-82.3913	-76.6764	-5.71494	0
4.	Myricitrin	-108.992	-79.9469	-29.0448	0	-87.1763	-73.3057	-13.8706	0
5.	Arjunolic acid	-95.3887	-81.6511	-13.425	-0.312637	-86.1421	-78.8447	-5.99124	-1.3061
6.	Celecoxib	-86.9344	-80.4249	-6.50946	0	-77.6205	-76.2528	-1.36773	0

Odd values indicate good binding energies. vDW: van der Waals energy; HB: hydrogen bonding energy; E.I.: electrostatic energy.

3.5.3. Molecular Dynamic (MD) Simulation

In the current investigation, the docking analysis was carefully monitored, and a few ligand protein complexes with the greatest interaction were selected. Thus, myricetin and myricitrin showed the highest interaction with cyclooxygenase 1 enzyme, while myricanone showed the highest interaction with TNF- α . The goal of the MD simulation was to determine the stability of compounds that interacted with different proteins. Thus, two different MD simulation tools, LARMD online tool and Schrodinger maestro software, were used in the present study. The LARMD molecular dynamic simulation result was explained in Supplementary File S1.

3.5.4. Schrodinger Molecular Dynamic Simulation

3.5.4.1. Stability Analysis of Complex by RMSD

Structural changes of the C α atoms were first calculated separately for each time point during the RMSD study for the MD simulation of PDB ID-4O1Z COX-1 (Figure 4A), COX-1 (Figure 4B), and PDB ID 2AZ5 TNF alpha (Figure 4C) with ligands myricetin, myricitrin, and myricanone. The RMSD analysis of proteins provides information about the rotational displacement of atoms in the PDB ID-4O1Z COX-1 (Figure 4A), COX-1 (Figure 4B), and PDB ID-2AZ5 TNF alpha (Figure 4C) structures throughout the course of 100 MD simulations. The RMSD analysis of the ligand provides information about the amino acid that interacts with the protein for ligand stability. The RMSD graph of PDB ID-4O1Z COX-1 (Figure 4A) illustrates the initial displacement of protein C α atoms, although it remained in the equilibrium phase until the simulation was completed, with an RMSD value ranging from 1.07–2.3 Å. While the ligand RMSD which ranges from 0.193–1.885 Å demonstrates the better stability of a complex exhibiting equilibrated motion during the 100 ns MD simulation. Similarly, the RMSD graph of PDB ID 4O1Z COX-1 (Figure 4B) represented the initial displacement of the protein C α atom. Even so, it kept the equilibrium phase going, although the simulation ended with values 1.172–2.247 Å. The ligand RMSD value ranges between 1.493–3.972 Å showed good complex stability by equilibrium motion throughout 100 ns of MD simulation. The RMSD graph of PDB ID 2AZ5 TNF alpha (Figure 4C) represents the initial displacement of protein C α atoms, but it reached the equilibrium phase until the end of the simulation with RMSD values ranging from 1.377 to 3.457, whereas the ligand RMSD with values ranging from 0.378 to 1.267 demonstrates the good stability of complex by equilibrated motion during 100 ns MD simulation.

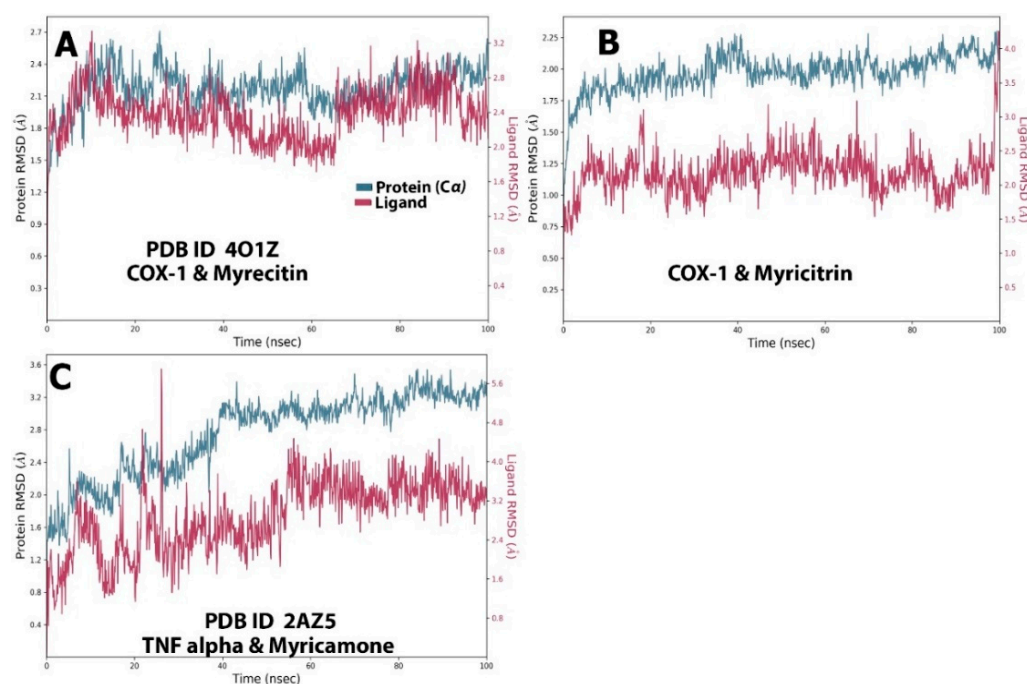


Figure 4. PDB ID-4O1Z COX-1 (A), COX-1 (B), and PDB ID 2AZ5 TNF alpha (C) with ligands myricetin, myricitrin, and myricanone. RMSD values plotted against simulation 100 ns.

A thorough examination of the RMSD of protein C α atoms for the PDB ID 2AZ5 TNF alpha protein reveals little time fluctuations. In the initial phase up to 10 ns, the RMSD value of protein C α atoms was 1.429–1.872 Å, after which it gets equilibrated with an RMSD value of 1.427–1.811 Å and again showed some fluctuation in the final 10 ns (90–100 ns) with an RMSD value of 1.853–2.258 Å. The ligand position slightly shifted from its previous position to another position several times with an RMSD value of 0.378–1.267 Å. Similarly, Figure 4B shows that the ligand RMSD value fluctuated at the end phase of the simulation of 5 ns (95–100 ns) ranging from 2.347–3.628 Å. On analysis with both the RMSD value the complexes PDB ID-4O1Z COX-1-myricetin and myricitrin and PDB ID 2AZ5 TNF alpha—myricanone, the result showed that PDB ID-4O1Z COX-1-myricetin was more stable system than PDB ID 2AZ5 TNF alpha—myricanone and PDB ID 4O1Z-COX-1-myricitrin, respectively.

3.5.4.2. Stability Analysis by RMSF

All C α atoms were subjected to the RMSF analysis for structural flexibility for each time point throughout the simulation for PDB ID-4O1Z COX-1-myricetin, PDB ID-4O1Z COX-1-myricitrin, and PDB ID 2AZ5 TNF alpha—myricanone. (Figure 5A–C). To elucidate the local conformational shift of the complex, RMSF analysis of the PDB ID-4O1Z COX-1 and PDB ID-2AZ5 TNF alpha structure RMSF has been conducted. During PDB ID-4O1Z COX-1-myricetin and myricitrin simulation, the peaks in the graph RMSF illustrate the fluctuation of C α . A and B, more profound analyses of the secondary structure of protein RMSF display the enhanced flexibility in the loop region followed by the beta-strand, and the alpha helix was more stable. The myricetin and myricitrin interact with PDB ID-4O1Z COX-1, mainly in the region of alpha-helices amino acids, so it displays good stability similar to alpha helices (green lines). The RMSF values of amino acids interacting with myricetin and myricitrin are 0.428–3.749 and 0.486–3.751 Å, respectively. These interacting residues allow the myricetin and myricitrin to explore the PDB ID-4O1Z COX-1 binding site to find a favorably energetic location to interact with the surrounding residue.

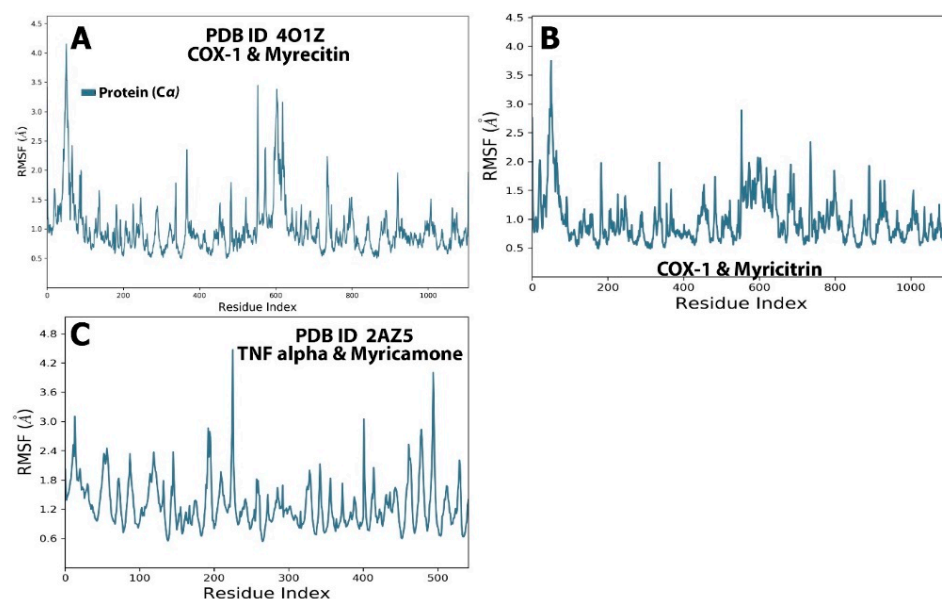


Figure 5. The PDB ID-4O1Z COX-1 (A), COX-1 (B), and PDB ID 2AZ5 TNF alpha (C) RMSF graph displays protein residue fluctuations from the 100 ns simulation (light blue curve) residues in interaction with the ligand.

The RMSF study of COX-1 indicates that all areas of the protein are flexible, with the exception of the myricanone-binding amino acid domains. The RMSF value of myricanone binding amino acids was found to be 0.536–4.472 Å whereas the RMSF value of protein was 0.536–4.472 Å; these values revealed that myricanone shows good binding affinity with protein, but due to the local fluctuation of c-alpha atoms of protein RMSD, values of myricanone displayed more variation.

3.5.4.3. Protein-Ligand Contact Analysis

In order to verify and examine the time-dependent interaction of protein-ligand complexes, as well as establish the complex's stabilization, a dynamic molecular study was carried out. The selection of best-docked complexes was made to execute MD simulations based on the findings of interaction research carried out on COX-1 and TNF- α with myricetin, myricitrin, and myricanone. The dynamic stability of complexes was characterized and evaluated using computational variables such as P-RMSF, protein-ligand RMSD, protein-ligand contacts, P-RMSF, ligand torsion profile, and ligand characteristics during a 100 ns MD simulation.

Monitoring the protein-ligand interaction was performed throughout the MD simulation. As shown in Figure 6A, myricetin was found to form hydrogen bonds directly with COX-1 at amino acid positions A:Ser143, A:Asn144, A:Arg374, A:Asn375, A:Arg376, B:Phe142, B:Leu224, B:His226, B:Gly227, B:Arg374, B:Asn375, and B:Gly536. Amino acid Asn375 present on the B chain of COX-1 protein was found to interact for approximately 0.85 interaction fraction. However, Leu224 and His226 formed hydrogen bonds for a 0.6 interaction fraction.

Furthermore, in Figure 6B, myricitrin formed hydrogen bonds at positions A:Ser143, A:Asn144, A:Val145, A:Leu224, A:Gly225, A:Arg374, A:Asn375, B:Ser143, B:Gly225, B:Arg374, B:Asn375, and B:Arg376 in COX-1 protein. The ligand was found to interact with the protein for approximately 2.3 interaction fraction of time. Figure 6C shows that myricanone formed hydrogen bonds at amino acid positions C:Ser60, C:Gln61, C:Leu120, C:Gly121, C:Tyr151, D:Ser60, and D:Leu120. The hydrogen bond formed by Leu120 in the D chain of TNF- α protein stabilized for about 0.4 of the interaction fraction time. All three ligands also formed hydrophobic and ionic interactions with different amino acids, as depicted in Figure 6.

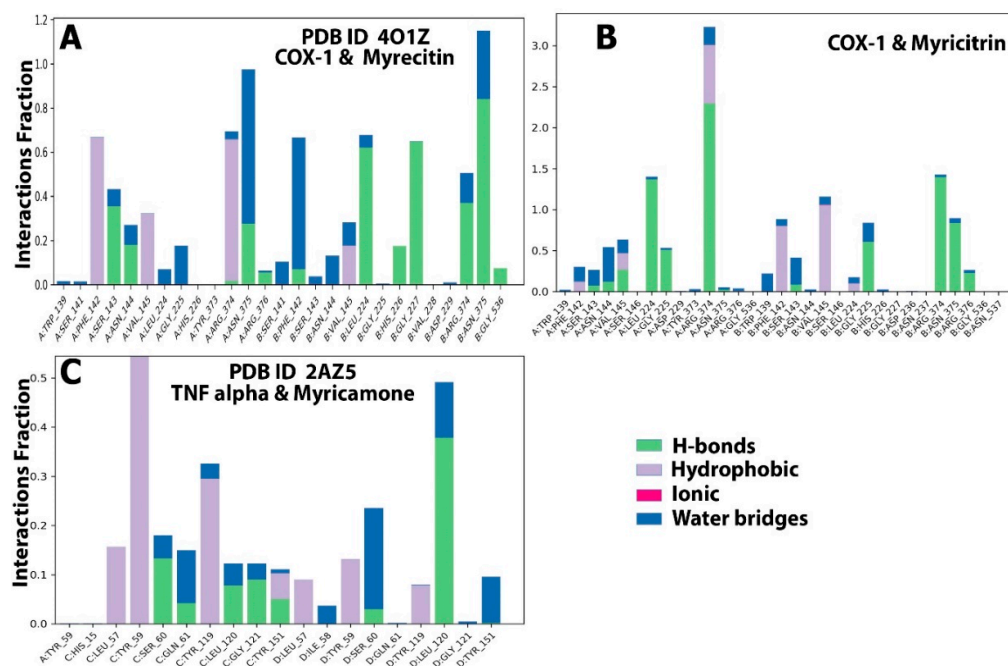


Figure 6. Protein-ligand contacts of (A) COX-1 and myrecitin, (B) COX-1 and myricitrin, and (C) TNF- α and myricanone during 100 ns simulation run.

COX-1 B:Asn375 and B:Gly:225 formed direct bonds with the OH-group of myricitrin for approximately 81% and 60% of the simulation run (Figure 6A). Additionally, A:Leu224 formed direct bonds with OH-groups for 48%, 55%, and 32% of the time of the run. However, A:Gly225 formed a direct bond with the OH-group for 50% of the run time. A:Arg374 formed bonds with OH-groups for 32% and 81%, whereas it formed bonds with the O-group for approximately 112% of the run time. Additionally, A:Arg374 formed pi-pi interaction with one of the benzene rings for 65% of the 100 ns simulation run time.

In the case of myricetin, three OH-groups formed direct bonds with A:Ser143, B:Gly227, B:Leu224, and B:Asn375 residues of COX-1 for approximately 35%, 64%, 60%, and 58% of the simulation run time, respectively. However, two other OH-groups formed water-mediated bonds with A:Asn375 for 33% and 34% of the run time. Additionally, two pi-pi bonds, one with A:Phe142 and the other with A:Arg374, were observed bonding with the two benzene rings of myricetin for 45% and 47% of the 100 ns run time. Furthermore, myricanone was found to form one direct bond with D:Leu120 residue of TNF alpha protein (Figure 7).

The radius of gyration (rGyr) provides a detailed indication of the compactness of the selected target protein structures with ligands. The myricetin-COX-1, myricitrin-COX-1, and myricanone- TNF alpha complexes ranged between 3.783–3.891 Å, 4.102–4.345 Å, and 3.358–3.662 Å, respectively. However, the number of intra-hydrogen bonds ranges between 0–2 for myricitrin-COX-1, myricetin-COX-1, and 0–1 for myricanone- TNF. The solvent-accessible surface area (SASA) helps determine how well the ligand and solvent interact during the complete simulation runtime. In the current study, the values of SASA range between 9.258–48.928 Å² for the myricetin-COX-1 complex, and 11.428–123.515 Å² for the myricitrin-COX-1 complex; however, values range between 64.599–233.373 Å² for the myricanone-TNF alpha complex. The solvent-accessible surface area of ligands with contributions from solely oxygen and nitrogen atoms was also measured using a polar surface. Furthermore, the molecular surface area (MolSA) was also calculated with a 1.4 Å probe radius that was equivalent to van der Waals surface area ranging between 355.514–372.228 Å² for myricitrin-COX-1, and 312.612–332.148 Å² and 310.953–327.422 Å² for myricanone-TNF alpha (Figure 8A–C), respectively.

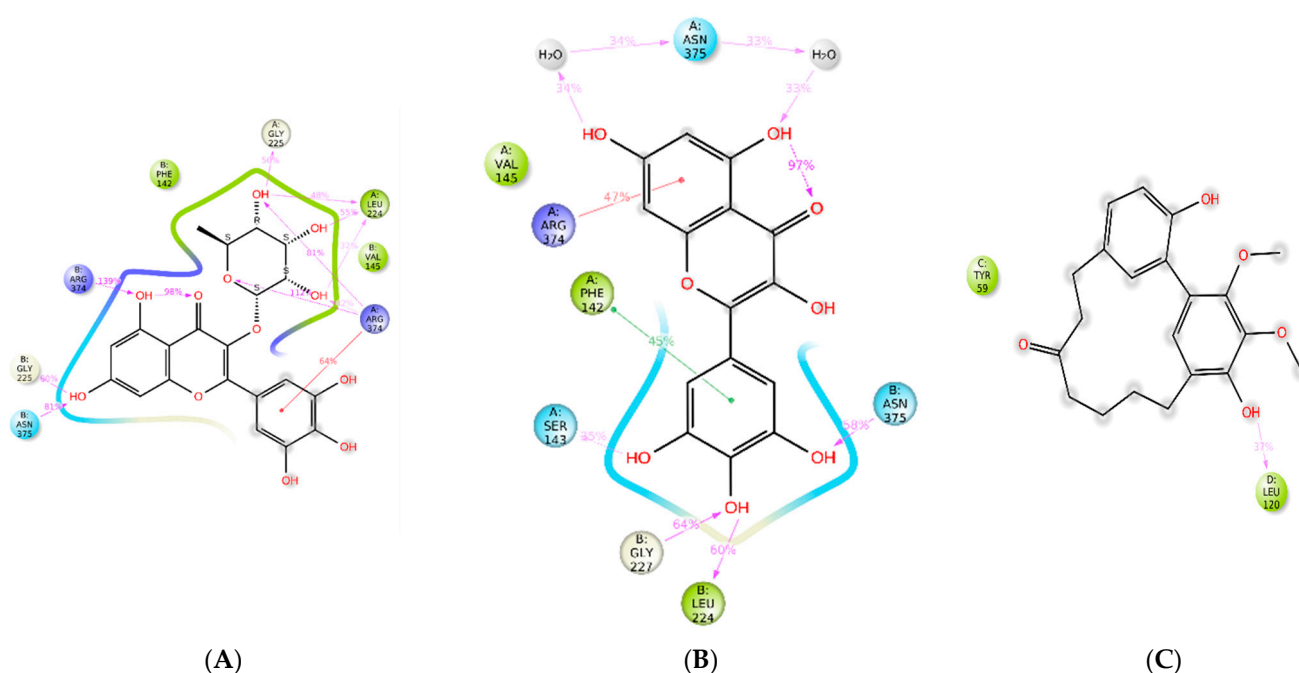


Figure 7. Ligand-protein contact analysis of (A) myricitrin with COX-1 protein (B) myricitrin with COX-1 protein and (C) myricanone with TNF alpha protein.

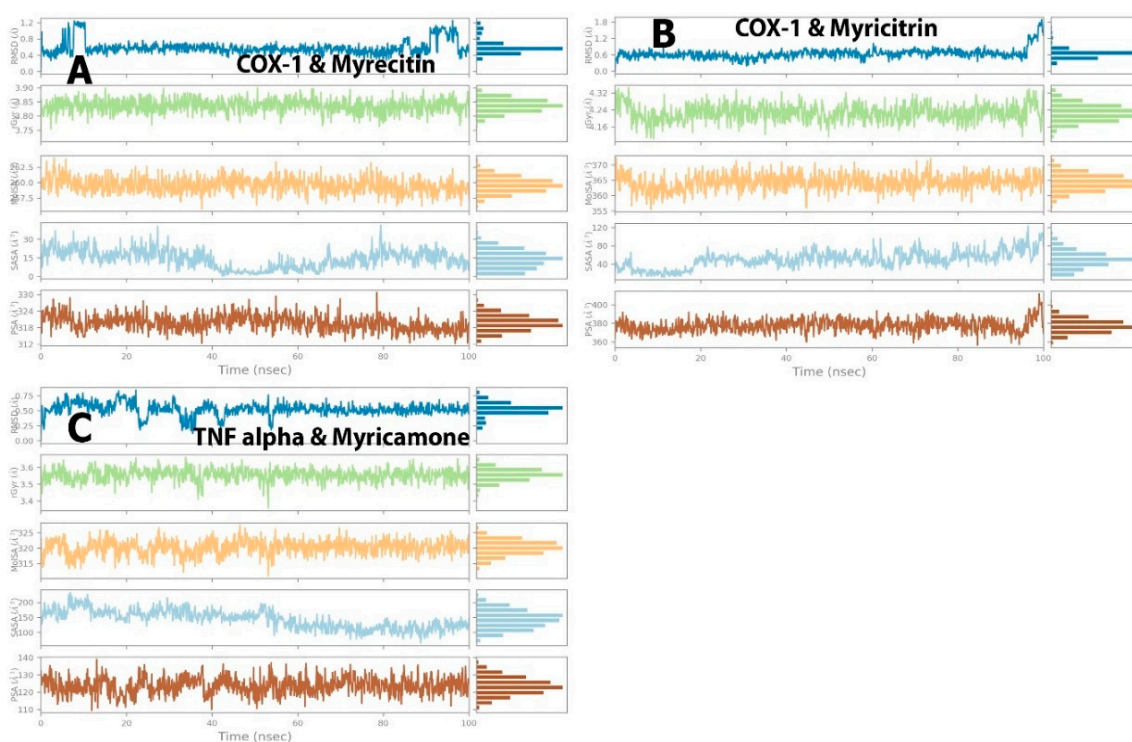


Figure 8. Ligand properties demonstrated of (A) myricitrin, (B) myricitrin, (C) myricanone by RMSD (blue line), radius of gyration (green line), molecular surface area (orange line), solvent accessible surface area (cyan blue line), and polar surface area (brown line).

4. Discussion

Extracts from *Myrica esculenta* have been reported to possess anti-allergic [41], anti-asthmatic [8], analgesic, anti-inflammatory, antipyretic [42,43], and mast cell-stabilizing properties [44]. Based on these shards of evidence, an effort has been undertaken to explore the anti-inflammatory property of certain compounds present in *M. esculenta* through

computational methods. The current study aimed to evaluate the *in vitro* anti-inflammatory activity of the aqueous extract of the bark and root of *M. esculenta* as well as *in silico* evaluation of selected phytoconstituents of *Myrica esculenta* (myricetin, myricanone, 3-epi-ursonic acid, myricitrin, arjunolic acid) against four inflammatory proteins (COX-1, COX-2, TNF- α , and IL-10) regarding the standard drug celecoxib.

Previous research showed that *M. esculenta* methanolic bark extract has the highest extractive values, 26.45% and 19.02%, respectively [45,46]. Similarly, in the present study, aqueous bark and root of *M. esculenta* showed similar extractive values of 24.76% and 21.92%, respectively.

A prior study by Kabra A. et al. claimed that aqueous leaves extract of *M. esculenta* showed significant total phenolic and flavonoid content of 62.38 ± 0.14 mg/g GAE and 35.77 ± 0.14 mg/g QE, respectively [10]. In this investigation, the aqueous bark and root extract of *M. esculenta* exhibited the greatest total phenolic (553.44 ± 18.38 , 226.02 ± 8.04 mg/g GAE) and flavonoid content (421.17 ± 5.34 , 277.65 ± 2.42 mg/g QE), respectively. A different prior study found that methanolic fruit pulp extract of *M. esculenta* contains a significant quantity of total phenolic and flavonoid content, which was 1.78 mg/g GAE and 1.59 mg/g QE, respectively [47]. Comparing different parts of the plant and their solvent, the present study showed the highest total phenolic and flavonoid content in the aqueous bark extract of *M. esculenta*.

Myrica rubra is a Chinese bayberry of the same family as *Myrica esculenta*. The previous study reported that aqueous leaves extract of *M. rubra* revealed a significant lipoxygenase inhibitory activity of IC₅₀ 50.57 μ g/mL [48]. Another earlier study conducted by Middha SK et al. found that the methanolic extract of *Myrica nagi* showed dose-dependent inhibition of IL-1 β and TNF- α . A 200 mg of *M. nagi* methanolic extract showed the highest inhibition in both inflammatory proteins [17]. In the current study, lipoxygenase enzyme activity was carried out, and a dose-dependent inhibition by the aqueous extract of *M. esculenta* was observed. As such, no previous lipoxygenase inhibitory activity of *M. esculenta* study was reported.

Molecular docking analysis of selected phytoconstituents using AutoDock4.2.6 has revealed that myricetin (BE = -9.95 kcal/mol, k_d = 50.71 nM) has excellent binding affinities with COX-1 (PDB ID: 4O1Z) followed by arjunolic acid (BE = -9.25 kcal/mol, k_d = 165.34 nM). Similar results were found using AutoDock vina.

In the case of binding affinities towards COX-2 (PDB ID: 4M11), myricetin (BE = -6.97 kcal/mol, k_d = 7.79 μ M) followed by arjunolic acid (BE = -6.92 kcal/mol, k_d = 8.5 μ M) exhibited best binding affinities as analyzed by AutoDock 4.2.6. The current results are in agreement with the docking score of myricetin and COX-2 protein (PDB ID: 4PH9) (BE = -6.52 kcal/mol) with a previous study performed by Kumar et al., 2019 [49]. In contrast, myricanone (BE = -10.5 kcal/mol, k_d = 13.51 M) displayed the greatest binding affinity with COX-2 protein as analyzed by AutoDock vina.

Likewise, in the case of binding interaction with TNF- α , myricanone (BE = -7.78 kcal/mol, k_d = 2.0 μ M) showed the best result, followed by arjunolic acid (BE = -7.34 kcal/mol, k_d = 4.2 μ M) (Table 6). However, the AutoDock vina analyzed result showed the best binding affinity arjunolic acid (BE = -9.4 kcal/mol, k_d = 120 nM) with TNF- α followed by 3-epi-ursonic acid (BE = -9.2 kcal/mol, k_d = 181.81 nM).

Similarly, myricanone showed the highest affinity towards IL-10 (PDB ID: 2H24) (BE = -7.09 kcal/mol, k_d = 6.32 μ M), as analyzed from AutoDock 4.2.6 (Table 6), whereas the AutoDock vina analyzed result exhibiting arjunolic acid (BE = -8.3 kcal/mol, k_d = 8848.93 nM) has the best affinity towards IL-10.

As is evident from the above results, the binding affinity of phytoconstituents showed modest variances, which might be attributed to discrepancies in grid box creation and identification of binding sites on target proteins by this software due to slight variations in the selection criterion. Because of this, the COX-1, COX-2, TNF-, and IL-10 proteins' binding pockets have different interactions with amino acids.

Based on binding energies and dissociation constant (K_d) values, myricetin, arjunolic acid, myricanone, and myricitrin were the most effective anti-inflammatory phytoconstituents in *Myrica esculenta*.

A molecular dynamics simulation is an important tool for understanding the dynamic behavior of a macromolecule in a biological system at various timeframes. RMSD is always a positive number, and a value of 0 indicates a perfect match to the data, which is impossible to attain in practice. Generally, a lower value of RMSD indicates a model is better than the target structure. When a dynamic system varies around a well-defined average location, the RMSD is referred to as the RMSF. Interestingly, in the present study, complexes of myricetin with COX-1, myricitrin, and COX-1 and myricanone with TNF- α protein were found to display very low deviations of 0.24–1.30 Å, 0.6–1.55 Å, and 0.44–1.35 Å, respectively, in a timeframe of 3 ns, which suggested good stability of complexes. Similarly, the analysis of RMSF, Rg, and Qx throughout 3 ns, comprising B-factors, demonstrated the thermodynamic stability of the above complexes. Similar to this, the study of a 100 ns MD simulation revealed that the RMSD values of myricetin COX-1, myricitrin COX-1, and myricanone TNF- α showed good stability and that their respective equilibrium motion ranges were 1.07–2.3 Å, 1.172–2.247 Å, and 1.493 Å, respectively. However, the myricetin COX-1 complex showed the highest RMSD and RMSF stability compared to other complexes.

5. Conclusions

In the current study, the aqueous extract of *M. esculenta* showed significant and dose-dependent antioxidant and anti-inflammatory activity. The result from the present study revealed that *M. esculenta* extract contains high TPC and TFC content, representing a major contributor to antioxidant capacity. Similarly, the bark and root extract of *M. esculenta* extract showed significant anti-inflammatory activity. The present study concluded that bark extract contains different types of bioactive compounds and revealed the highest antioxidant and anti-inflammatory activity compared to root extract.

Supplementary Materials: The following supporting information and presentation material can be downloaded at: <https://www.mdpi.com/article/10.3390/ECB2023-14079/s1>, supporting information: (1) Best docking poses of selected phytoconstituents of *Myrica esculenta* with COX-1, COX-2, TNF-alpha and interleukin 10 generated by using AutoDock 4.2.6, AutoDock Vina and iGEMDOCK. (2) Molecular dynamic (MD) simulation study by using LARMD online server.

Author Contributions: Conceptualization, A.K.S. and D.C.; methodology, D.C. and L.S.; Software, A.K.S., D.C., M.A., M.E.A., S.T.A.-S. and W.A.E.; validation, A.K.S., P.P.G. and M.P.; formal analysis, A.K.S., D.C. and A.G.; investigation, A.K.S. and M.A.; resources, D.C.; data curation, D.C. and A.K.S.; writing original, D.C., A.T., A.P., A.S. and A.K.S.; draft preparation, A.K.S., D.C., P.P.G. and M.P.; writing review and editing, A.P., A.T. and A.S.; supervision, A.K.S., L.S., A.P. and P.P.G. All authors have read and agreed to the published version of the manuscript.

Funding: This research received no external funding.

Institutional Review Board Statement: Before starting the experiment, the research proposal was submitted to the Institutional Review committee (IRC). After taking the approval from the (IRC) the experiments were started. The IRC Registration No UCMS/IRC/187/22.

Informed Consent Statement: Not applicable.

Data Availability Statement: Not applicable.

Acknowledgments: The authors extend their appreciation to the Researchers Supporting Project number (RSPD2023R543), King Saud University, Riyadh, Saudi Arabia.

Conflicts of Interest: The authors have no conflict of interest.

References

- Min, Z.; Navam, S.H.; Ronny, H.; Arvind, K.; Apputhury, P.M.; Arumugam, M.; Rasekhara, R.M. Phytochemicals, antioxidant and antimicrobial activity of *Hibiscus sabdariffa*, *Centella asiatica*, *Moringa oleifera* and *Murraya koenigii* leaves. *J. Med. Plants Res.* **2011**, *5*, 6672–6680.
- Utami, W.; Aziz, H.; Fitriani, I.; Zikri, A.; Mayasri, A.; Nasrudin, D. In silico anti-inflammatory activity evaluation of some bioactive compound from *Ficus religiosa* through molecular docking approach. *J. Phys. Conf. Ser.* **2020**, *1563*, 012024. [\[CrossRef\]](#)
- Ul Hassan, S.S.; Zhang, W.-D.; Jin, H.-Z.; Basha, S.H.; Priya, S.S. In silico anti-inflammatory potential of guaiane dimers from *Xylopia vielana* targeting COX-2. *J. Biomol. Struct. Dyn.* **2022**, *40*, 484–498. [\[CrossRef\]](#) [\[PubMed\]](#)
- Dinarello, C.A. Anti-inflammatory agents: Present and future. *Cell* **2010**, *140*, 935–950. [\[CrossRef\]](#) [\[PubMed\]](#)
- Oboh, G. Effect of blanching on the antioxidant properties of some tropical green leafy vegetables. *LWT Food Sci. Technol.* **2005**, *38*, 513–517. [\[CrossRef\]](#)
- Refaey, M.S.; Abouelela, M.E.; El-Shoura, E.A.M.; Alkhalidi, H.M.; Fadil, S.A.; Elhady, S.S.; Abdelhameed, R.F.A. In Vitro Anti-Inflammatory Activity of *Cotula anthemoides* Essential Oil and In silico Molecular Docking of Its Bioactives. *Molecules* **2022**, *27*, 1994. [\[CrossRef\]](#) [\[PubMed\]](#)
- Tiwari, M.; Dwivedi, U.N.; Kakkar, P. Suppression of oxidative stress and pro-inflammatory mediators by *Cymbopogon citratus* D. Stapf extract in lipopolysaccharide stimulated murine alveolar macrophages. *Food Chem. Toxicol.* **2010**, *48*, 2913–2919. [\[CrossRef\]](#)
- K Rana, R.; K Patel, R. Pharmacological evaluation of antiasthmatic activity of *Myrica nagi* bark extracts. *Anti-Inflamm. Anti-Allergy Agents Med. Chem.* **2016**, *15*, 145–152. [\[CrossRef\]](#)
- Kabra, A.; Martins, N.; Sharma, R.; Kabra, R.; Baghel, U.S. *Myrica esculenta* Buch.-Ham. ex D. Don: A Natural Source for Health Promotion and Disease Prevention. *Plants* **2019**, *8*, 149. [\[CrossRef\]](#)
- Kabra, A.; Sharma, R.; Hano, C.; Kabra, R.; Martins, N.; Baghel, U.S. Phytochemical Composition, Antioxidant, and Antimicrobial Attributes of Different Solvent Extracts from *Myrica esculenta* Buch.-Ham. ex. D. Don Leaves. *Biomolecules* **2019**, *9*, 357. [\[CrossRef\]](#)
- Sood, P.; Shri, R. A review on ethnomedicinal, phytochemical and pharmacological aspects of *Myrica esculenta*. *Indian J. Pharm. Sci.* **2018**, *80*, 2–13. [\[CrossRef\]](#)
- Fang, Z.; Zhang, Y.; Lü, Y.; Ma, G.; Chen, J.; Liu, D.; Ye, X. Phenolic compounds and antioxidant capacities of bayberry juices. *Food Chem.* **2009**, *113*, 884–888. [\[CrossRef\]](#)
- Srivastava, B.; Sharma, V.C.; Pant, P.; Pandey, N.; Jadhav, A. Evaluation for substitution of stem bark with small branches of *Myrica esculenta* for medicinal use—A comparative phytochemical study. *J. Ayurveda Integr. Med.* **2016**, *7*, 218–223. [\[CrossRef\]](#) [\[PubMed\]](#)
- Mahato, R.; Chaudhary, R. Ethnomedicinal study and antibacterial activities of selected plants of Palpa district, Nepal. *Sci. World* **2005**, *3*, 26–31.
- Rauf, A.; Abu-Izneid, T.; Rashid, U.; Alhumaydhi, F.A.; Bawazeer, S.; Khalil, A.A.; Aljohani, A.S.M.; Abdallah, E.M.; Al-Tawaha, A.R.; Mabkhot, Y.N.; et al. Anti-inflammatory, Antibacterial, Toxicological Profile, and In silico Studies of Dimeric Naphthoquinones from *Diospyros lotus*. *Biomed Res. Int.* **2020**, *2020*, 7942549. [\[CrossRef\]](#)
- Singh, J.; Lan, V.K.; Trivedi, V.P. Pharmacognostic Evaluation of *Katphala* (The bark of *Myrica esculenta* Buch—Ham). *Anc. Sci. Life* **1986**, *6*, 85–87.
- Middha, S.K.; Usha, T.; Babu, D.; Misra, A.K.; Lokesh, P.; Goyal, A.K. Evaluation of antioxidative, analgesic and anti-inflammatory activities of methanolic extract of *Myrica nagi* leaves-an animal model approach. *Symbiosis* **2016**, *70*, 179–184. [\[CrossRef\]](#)
- Yadav, D.K.; Mudgal, V.; Agrawal, J.; Maurya, A.K.; Bawankule, D.U.; Chanotiya, C.S.; Khan, F.; Thul, S.T. Molecular docking and ADME studies of natural compounds of Agarwood oil for topical anti-inflammatory activity. *Curr. Comput. Aided Drug. Des.* **2013**, *9*, 360–370. [\[CrossRef\]](#)
- Wang, Y.; Hu, B.; Peng, Y.; Xiong, X.; Jing, W.; Wang, J.; Gao, H. In silico exploration of the molecular mechanism of cassane diterpenoids on anti-inflammatory and immunomodulatory activity. *J. Chem. Inf. Model.* **2019**, *59*, 2309–2323. [\[CrossRef\]](#)
- Iqbal, D.; Khan, M.S.; Waiz, M.; Rehman, M.T.; Alaidarous, M.; Jamal, A.; Alothaim, A.S.; AlAjmi, M.F.; Alshehri, B.M.; Banawas, S. Exploring the Binding Pattern of Geraniol with Acetylcholinesterase through In silico Docking, Molecular Dynamics Simulation, and In Vitro Enzyme Inhibition Kinetics Studies. *Cells* **2021**, *10*, 3533. [\[CrossRef\]](#)
- Kabra, A.; Sharma, R.; Singla, S.; Kabra, R.; Baghel, U.S. Pharmacognostic characterization of *Myrica esculenta* leaves. *J. Ayurveda Integr. Med.* **2019**, *10*, 18–24. [\[CrossRef\]](#) [\[PubMed\]](#)
- Chludil, H.D.; Corbino, G.B.; Leicach, S.R. Soil quality effects on *Chenopodium album* flavonoid content and antioxidant potential. *J. Agric. Food Chem.* **2008**, *56*, 5050–5056. [\[CrossRef\]](#) [\[PubMed\]](#)
- Shrivastava, A.K.; Thapa, S.; Shrestha, L.; Mehta, R.K.; Gupta, A.; Koirala, N. Phytochemical screening and the effect of *Trichosanthes dioica* in high-fat diet induced atherosclerosis in Wistar rats. *Food Front.* **2021**, *2*, 527–536. [\[CrossRef\]](#)
- Olivia, N.U.; Goodness, U.C.; Obinna, O.M. Phytochemical profiling and GC-MS analysis of aqueous methanol fraction of *Hibiscus asper* leaves. *Future J. Pharm. Sci.* **2021**, *7*, 59. [\[CrossRef\]](#)
- Truong, D.H.; Ta, N.T.A.; Pham, T.V.; Huynh, T.D.; Do, Q.T.G.; Dinh, N.C.G.; Dang, C.D.; Nguyen, T.K.C.; Bui, A.V. Effects of solvent—Solvent fractionation on the total terpenoid content and in vitro anti-inflammatory activity of *Serevenia buxifolia* bark extract. *Food Sci. Nutr.* **2021**, *9*, 1720–1735. [\[CrossRef\]](#)
- Paun, G.; Neagu, E.; Albu, C.; Savin, S.; Radu, G.L. In vitro evaluation of antidiabetic and anti-inflammatory activities of polyphenolic-rich extracts from *anchusa officinalis* and *melilotus officinalis*. *ACS Omega* **2020**, *5*, 13014–13022. [\[CrossRef\]](#)

27. Ahmad, R. Steroidal glycoalkaloids from *Solanum nigrum* target cytoskeletal proteins: An In silico analysis. *PeerJ* **2019**, *7*, 6012. [\[CrossRef\]](#)
28. Contreras-Puentes, N.; Alviz-Amador, A. Virtual screening of natural metabolites and antiviral drugs with potential inhibitory activity against 3CL-PRO and PL-PRO. *Biomed. Pharmacol. J.* **2020**, *13*, 933–941. [\[CrossRef\]](#)
29. Khan, T.; Azad, I.; Ahmad, R.; Raza, S.; Dixit, S.; Joshi, S.; Khan, A.R. Synthesis, characterization, computational studies and biological activity evaluation of Cu, Fe, Co and Zn complexes with 2-butanone thiosemicarbazone and 1, 10-phenanthroline ligands as anticancer and antibacterial agents. *Excli J.* **2018**, *17*, 331.
30. Okoli, B.J.; Eltayb, W.A.; Gyebi, G.A.; Ghanam, A.R.; Ladan, Z.; Oguegbulu, J.C.; Abdalla, M. In silico Study and Excito-Repellent Activity of *Vitex negundo* L. Essential Oil against *Anopheles gambiae*. *Appl. Sci.* **2022**, *12*, 7500. [\[CrossRef\]](#)
31. Mohapatra, R.K.; Dhama, K.; El-Arabey, A.A.; Sarangi, A.K.; Tiwari, R.; Emran, T.B.; Azam, M.; Al-Resayes, S.I.; Raval, M.K.; Seidel, V. Repurposing benzimidazole and benzothiazole derivatives as potential inhibitors of SARS-CoV-2: DFT, QSAR, molecular docking, molecular dynamics simulation, and In silico pharmacokinetic and toxicity studies. *J. King Saud. Univ. Sci.* **2021**, *33*, 101637. [\[CrossRef\]](#)
32. Alameen, A.A.; Abdalla, M.; Alshibl, H.M.; AlOthman, M.R.; Alkhulaifi, M.M.; Mirgany, T.O.; Elsayim, R. In silico studies of glutathione peroxidase4 activators as candidate for multiple sclerosis management. *J. Saudi Chem. Soc.* **2022**, *26*, 101554. [\[CrossRef\]](#)
33. Morris, G.M.; Goodsell, D.S.; Halliday, R.S.; Huey, R.; Hart, W.E.; Belew, R.K.; Olson, A.J. Automated docking using a Lamarckian genetic algorithm and an empirical binding free energy function. *J. Comput. Chem.* **1998**, *19*, 1639–1662. [\[CrossRef\]](#)
34. Trott, O.; Olson, A.J. AutoDock Vina: Improving the speed and accuracy of docking with a new scoring function, efficient optimization, and multithreading. *J. Comput. Chem.* **2010**, *31*, 455–461. [\[CrossRef\]](#) [\[PubMed\]](#)
35. Yang, J.M.; Chen, C.C. GEMDOCK: A generic evolutionary method for molecular docking. *Proteins* **2004**, *55*, 288–304. [\[CrossRef\]](#) [\[PubMed\]](#)
36. Dolinsky, T.J.; Czodrowski, P.; Li, H.; Nielsen, J.E.; Jensen, J.H.; Klebe, G.; Baker, N.A. PDB2PQR: Expanding and upgrading automated preparation of biomolecular structures for molecular simulations. *Nucleic Acids Res.* **2007**, *35*, W522–W525. [\[CrossRef\]](#) [\[PubMed\]](#)
37. Yang, J.-F.; Wang, F.; Chen, Y.-Z.; Hao, G.-F.; Yang, G.-F. LARMD: Integration of bioinformatic resources to profile ligand-driven protein dynamics with a case on the activation of estrogen receptor. *Brief. Bioinform.* **2020**, *21*, 2206–2218. [\[CrossRef\]](#)
38. Kausar, M.A.; Anwar, S.; Eltayb, W.A.; Kuddus, M.; Khatoon, F.; El-Arabey, A.A.; Khalifa, A.M.; Rizvi, M.R.; Najm, M.Z.; Thakur, L.; et al. MD Simulation Studies for Selective Phytochemicals as Potential Inhibitors against Major Biological Targets of Diabetic Nephropathy. *Molecules* **2022**, *27*, 4980. [\[CrossRef\]](#)
39. Baby, K.; Maity, S.; Mehta, C.H.; Suresh, A.; Nayak, U.Y.; Nayak, Y. Targeting SARS-CoV-2 RNA-dependent RNA polymerase: An In silico drug repurposing for COVID-19. *F1000Research* **2020**, *9*, 1166. [\[CrossRef\]](#)
40. Trivedi, A.; Ahmad, R.; Siddiqui, S.; Misra, A.; Khan, M.A.; Srivastava, A.; Ahamad, T.; Khan, M.F.; Siddiqui, Z.; Afrin, G. Prophylactic and therapeutic potential of selected immunomodulatory agents from Ayurveda against coronaviruses amidst the current formidable scenario: An In silico analysis. *J. Biomol. Struct. Dyn.* **2022**, *40*, 9648–9700. [\[CrossRef\]](#)
41. Patel, K.; Rao, N.; Gajera, V.; Bhatt, P.; Patel, K.; Gandhi, T. Anti-allergic activity of stem bark of *Myrica esculenta* Buch.-Ham (Myricaceae). *J. Young Pharm.* **2010**, *2*, 74–78. [\[CrossRef\]](#)
42. Patel, T.; Dudhpejiya, A.; Sheath, N. Anti inflammatory activity of *Myrica nagi* Linn. Bark. *Anc. Sci. Life* **2011**, *30*, 100. [\[PubMed\]](#)
43. Patel, M. Analgesic and anti-inflammatory activity of ethanolic extract of stem bark of *Myrica nagi* (T.). *World J. Pharm. Res.* **2017**, *6*, 844–857. [\[CrossRef\]](#)
44. Patel, T.; Rajshekar, C.; Parmar, R. Mast cell stabilizing activity of bark of *Myrica nagi*. *J. Pharm. Stud. Res.* **2011**, *2*, 1–6.
45. Shresta, S.; Bhattarai, B.R.; Adhikari, B.; Rayamajhee, B.; Poudel, P.; Khanal, S.; Marasini, B.P.; Aryal, B.; Bhandari, S.; Parajuli, N. Evaluation of phytochemical, antioxidant and antibacterial activities of selected medicinal plants. *Nepal J. Biotechnol.* **2021**, *9*, 50–62. [\[CrossRef\]](#)
46. Anjum, N.; Tripathi, Y. evaluation of total polyphenols, flavonoids and antioxidant activity of *Myrica esculenta* buch-ham. ex d. don fruits. *World J. Pharm. Med. Res.* **2021**, *7*, 186–192.
47. Rawat, S.; Jugran, A.; Giri, L.; Bhatt, I.D.; Rawal, R.S. Assessment of antioxidant properties in fruits of *Myrica esculenta*: A popular wild edible species in Indian Himalayan region. *Evid. Based Complement. Altern. Med.* **2011**, *2011*, 512787. [\[CrossRef\]](#) [\[PubMed\]](#)
48. Langhansova, L.; Landa, P.; Kutil, Z.; Tauchen, J.; Marsik, P.; Rezek, J.; Lou, J.D.; Yun, Z.L.; Vanek, T. *Myrica rubra* leaves as a potential source of a dual 5-LOX/COX inhibitor. *Food Agric. Immunol.* **2017**, *28*, 343–353. [\[CrossRef\]](#)
49. Kumar, H.P.; Panda, P.; Karunakar, P.; Shiksha, K.; Singh, L.; Ramesh, N.; Usha, T.; Middha, S.K. Potential Cyclooxygenase (COX-2) enzyme inhibitors from *Myrica nagi*-from In silico to in vitro investigation. *Pharmacogn. Mag.* **2019**, *15*, 280.

Disclaimer/Publisher's Note: The statements, opinions and data contained in all publications are solely those of the individual author(s) and contributor(s) and not of MDPI and/or the editor(s). MDPI and/or the editor(s) disclaim responsibility for any injury to people or property resulting from any ideas, methods, instructions or products referred to in the content.